

Dynamic Mode Decomposition Analysis of Rotating Detonation Waves

Richard Bluemner, Myles D. Bohon, Christian Oliver Paschereit
Technische Universität Berlin
10623, Berlin, Germany
&
Ephraim J. Gutmark
University of Cincinnati
Cincinnati, OH, USA

1 Introduction

Rotating Detonation Combustors (RDCs) have emerged as one of the most promising concepts to harvest the efficiency gains made possible through Pressure Gain Combustion (PGC). In an RDC, a detonation wave constantly propagates around a closed-loop combustion annulus, while fresh reactants are constantly supplied from one end and product gases are expanded and displaced out of the other end. The simple design, together with the high power density, and low pressure fluctuations in the exhaust gas make them an ideal candidate for propulsive and land-based power applications [1].

Apart from the canonical single detonation wave mode, many groups have reported diverging wave modes, such as the steady operation with counter-rotating waves [2] and high-frequency longitudinal pulsed operation [3]. A recent study by the authors found that depending on the injector geometry and reactant mass flow rate, their RDC was able to stabilize many different operating modes, such as two counter-rotating waves at equal or different speed, a dominant wave with pairs or triplets of counter-rotating waves, as well as secondary acoustic or dominant pulsed wave modes [4]. These wave modes lead to complex pressure oscillations in the annulus that were analyzed based on the theoretical speed of sound in the fresh and hot gas, the detonation velocity, and observations from high-speed video.

This work aims to complement the previous studies and to provide a better understanding about the correlation between the pressure signals measured in the combustor annulus and the data contained in the high-speed aft end video. Towards this goal, the Dynamic Mode Decomposition (DMD) technique will be applied to these videos. To the knowledge of the authors, this is the first application of this technique to study aft end videos of RDC operation. The DMD technique was originally developed to extract dynamic information from a sequence of snapshots of a flow field [5]. Since its development, it has been applied in many different fields, including systems with non-linear dynamics, such as detonation waves [6]. In these non-linear systems, the DMD is able to extract the dominant dynamic behavior captured in the data sequence [5]. A comprehensive review of the technique is provided in [7].

2 Experimental Setup & Methodology

The RDC under investigation uses a radially-inward injector design, where air is injected through a narrow slot of variable height at the bottom of the annulus, and fuel (hydrogen) is injected through a large number of discretely spaced holes. Fuel and air mix in a jet-in-cross flow configuration. The RDC was ignited with a pre-detonator tube from the outer annulus wall near the injector head. Operation is computer-controlled and monitored by a 500 kHz data acquisition system. Run times were in the order of 300 ms to prevent sensor damage due to the high temperatures in the combustion zone. Dynamic pressure sensors (PCB112A05) were mounted in a recessed cavity in the annulus outer wall close to the combustion zone to measure the passage of the detonation wave, as well as any other pressure oscillations in the RDC annulus.

A high-speed camera (Photron SA-Z) was used to image the natural flame luminosity from the aft end of the RDC via a visible wavelength mirror. Since the mirror is non-reflective in the UV, the camera images the broad-band emission from the combustion products (primarily hot water) in the visible and near-IR spectrum. Images were recorded at a rate of 87500 frames per second, with an exposure time of $8.75 \mu\text{s}$ and an inter-frame time of $11.4 \mu\text{s}$. Images were constrained to a 200×200 pixel region, corresponding to approximately 2 pixels/mm. The high-speed images allow for an assessment of the number, direction, and location of the waves in the annulus. For many operating points, however, complex wave modes are observed where the distinction between individual waves becomes difficult.

The DMD analysis is applied to the high-speed videos to gain a deeper understanding of the different modes involved in the process of wave propagation. The DMD is a data-based approach, which only relies on snapshots of the flow [5]. This makes it an ideal tool to be applied here. Knowledge of the model describing the system is not necessary. Instead, the data is approximated as a linear combination of the DMD modes. The calculation of the DMD modes follows the standard method by Schmid [5], which solves the eigenvalue problem of a companion matrix based on the QR-decomposition of the snapshot matrix, the eigenvalues of which approximate the eigenvalues of the system matrix. In its standard application, the DMD is used to identify coherent structures in the flow and their corresponding growth and decay rates to differentiate between stable and unstable modes. However, in this application the DMD is used to separate the different steady modes that are contained in the luminosity signal. As a result, all identified modes are stable.

The DMD is performed on a sequence of 2500 frames of high-speed video, starting at a run time of 200 ms. At a camera frame rate of 87500 fps, this results in a captured time interval of $\Delta t = 28.57$ ms. Based on typically observed wave speeds in RDCs of 50-80% of Chapman-Jouguet (CJ) speed, between 100 and 170 full laps of a wave are captured. In order to exclude any modes occurring outside of the annulus, the views of the exhaust plume around the combustor and the center body are masked prior to the analysis. The annulus location is automatically detected in each frame by an image processing algorithm, as described in [8].

The DMD spectrum, which shows the norm of each mode as a function of frequency (i.e. the argument of the DMD eigenvalues), is compared to the pressure spectrum and the DMD modes are extracted at frequencies where both spectra overlap. For each of these modes, this yields a matrix of complex values that describe the magnitude and phase of the coherent fluctuations with the respective frequency at each pixel. The magnitude plot shows the strength of the mode at each pixel. The phase plot indicates the temporal development of the mode in the radial and azimuthal directions. Based on the phase distribution of each mode, the number of nodes and the dynamic behavior (e.g. rotating or longitudinal) can be analyzed. Depending on the operating mode, the number of nodes may indicate the number of propagating waves, as well as their higher harmonics (if a mode at an integer multiplier is observed).

3 Results

The results section is divided into three parts with each discussing a different operating mode, starting with two counter-rotating waves of equal speed, followed by two CR waves of different speeds, and concluding with the case of a dominant wave with a pair of counter-rotating waves.

3.1 Two Counter-Rotating Waves at Equal Speed (2CR)

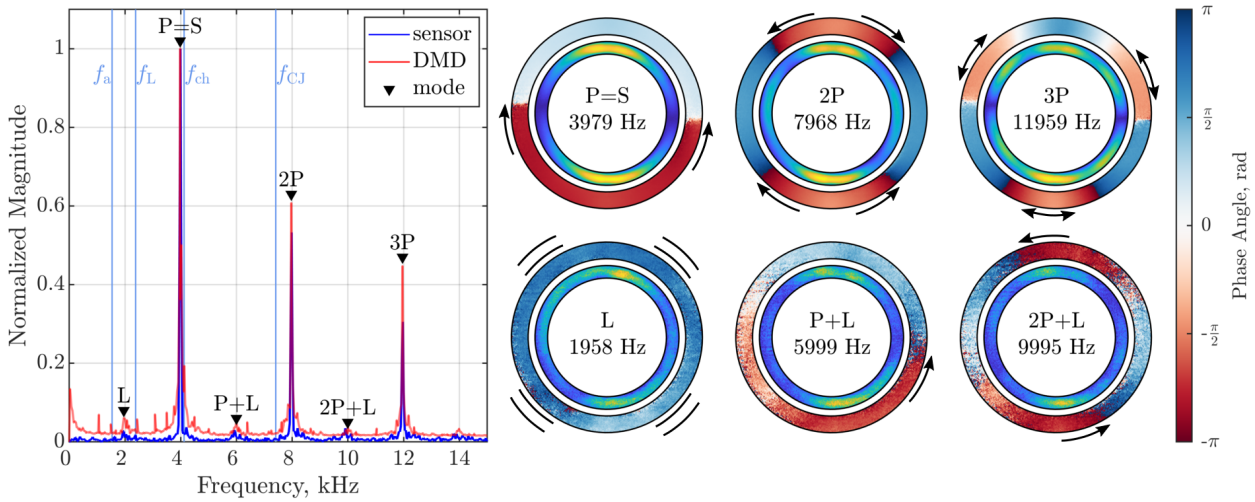


Figure 1: 2CR mode at air mass flow of 125 g/s and equivalence ratio of 0.9: (left) DMD and pressure spectrum, and (right) corresponding mode phase (outer circle) and magnitude (inner circle).

At low reactant mass flow rates, operating modes with two counter-rotating waves were observed. Previous analysis has shown that in these cases, both waves propagate at an equal speed close to the speed of sound in the products, which leads to a clapping wave mode with spatially locked wave intersection points [9].

On the left, Fig. 1 shows the spectrum of a pressure sensor mounted in the annulus wall close to the injector head (blue), and the DMD spectrum based on the high-speed video (red). Both spectra are normalized by the magnitude of the primary operating frequency. As a reference, the plot also includes frequencies of theoretical speeds for waves propagating at the speed of sound in the fresh reactants (f_a), at the speed of sound in the products (f_{ch}), and at CJ conditions (f_{CJ}). Previous work suggested that the RDC can also stabilize secondary longitudinal resonance modes related to the quarter-wave resonance frequency, based on the annulus length and the speed of sound in the products [4]. The corresponding frequency is indicated as f_L .

Both spectra agree well, indicating that the spectral peaks observed in the pressure signal are visible in the coherent luminosity changes. The relevant peaks in the pressure spectrum are marked and labeled according to the identified mode. On the right hand side of the figure, the resulting mode shapes are plotted in terms of their phase (outer circle) and magnitude (inner circle). All phase plots are scaled between $-\pi$ (red) and π (blue), while the magnitudes are scaled individually for each mode, with dark blue corresponding to zero magnitude. The figure at the top left shows the strongest mode in the system labeled as P=S, which corresponds to the clapping motion as a result of the locked wave intersection point between the two waves.

The arrows indicate the propagation direction of the two counter-rotating wave fronts, which result in a mode with two phase discontinuities or nodes. This also leads to a reflection symmetry phase split, as well as magnitude hot spots at the top and bottom of the annulus. This wave motion is observed as the dominant feature in the video. The next two modes labeled 2P and 3P show the second and third higher harmonic of the clapping mode, since they are observed at integer multiple frequencies of P. As a result, they have two and three times as many nodes compared to P, respectively. Their magnitudes appear more azimuthally distributed with higher harmonic order.

At the bottom left, the mode shape calculated at the spectral peak close to f_L shows a constant phase throughout the annulus, together with a slight magnitude increase at the wave intersection points. The phase plotted over time shows a global oscillation in the annulus without any distinct wave fronts. This indicates that this mode shows a longitudinal oscillation which is close to the quarter-wave frequency and is hence labeled as L. This longitudinal resonance leads to interaction modes with the rotating waves and their higher harmonics, at frequencies corresponding to P+L, as well as 2P+L. The corresponding mode shapes are also shown. Surprisingly, they describe a rotating motion of one and two nodes in counter-clockwise direction, respectively, which might be driven by twice L being at a slightly lower frequency than P.

3.2 Two Counter-Rotating Waves at Different Speed (2CRT)

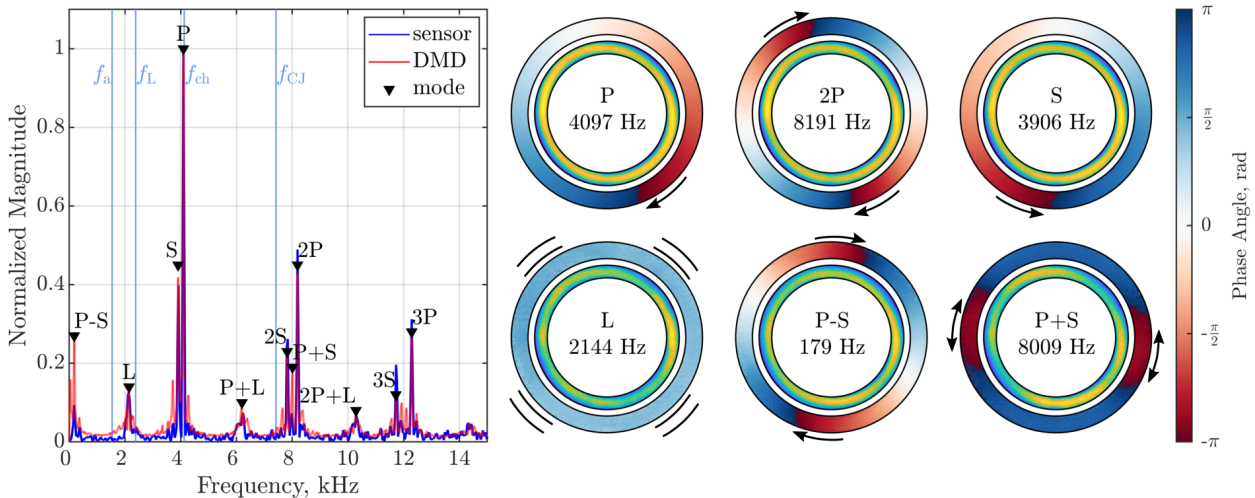


Figure 2: 2CRT mode at air mass flow of 150 g/s and equivalence ratio of 0.9: (left) DMD and pressure spectrum, and (right) corresponding mode phase (outer circle) and magnitude (inner circle).

When the reactant mass flow is increased, operation is observed to transition to two counter-rotating waves at different speeds. The resulting spectra and selected mode shapes are shown in Fig. 2. As in the previous case, the largest peak describes the dominant wave mode, which is a clockwise rotating primary wave, denoted as P. The magnitude is constant throughout the annulus, indicating a stable propagation of the wave. The second higher harmonic of the primary wave (labeled as 2P) shows two nodes propagating in the same direction as P. The same logic applies to the other higher harmonics. Just below P, the frequency peak corresponding to a single secondary wave S can be found. Consistent with the video, the mode shape on the right shows the counter-clockwise propagation of S at constant magnitude. Similar to the previous example,

this operating mode also shows the presence of an L mode, now at increased strength. The spectrum also shows additional features compared to the previous example. At the lower end, a relatively large peak was identified as the speed of the wave intersection point, equal to the difference between the speeds of P-S. As P is faster than S the intersection point rotates in the same direction as P. The influence of the wave intersection point in the magnitude of P is smeared out in this example, as it constantly propagates around the annulus due to the difference in individual wave speeds. In each cycle of the primary wave it intersects the secondary wave twice, leading to two nodes. The intersection frequency itself is found at the combined speed $P+S$ and shows the wave strengthening due to the intersection in dark red, similar to the 2P mode in the previous example.

3.3 Dominant Wave with Counter-Rotating Pair (D/S2)

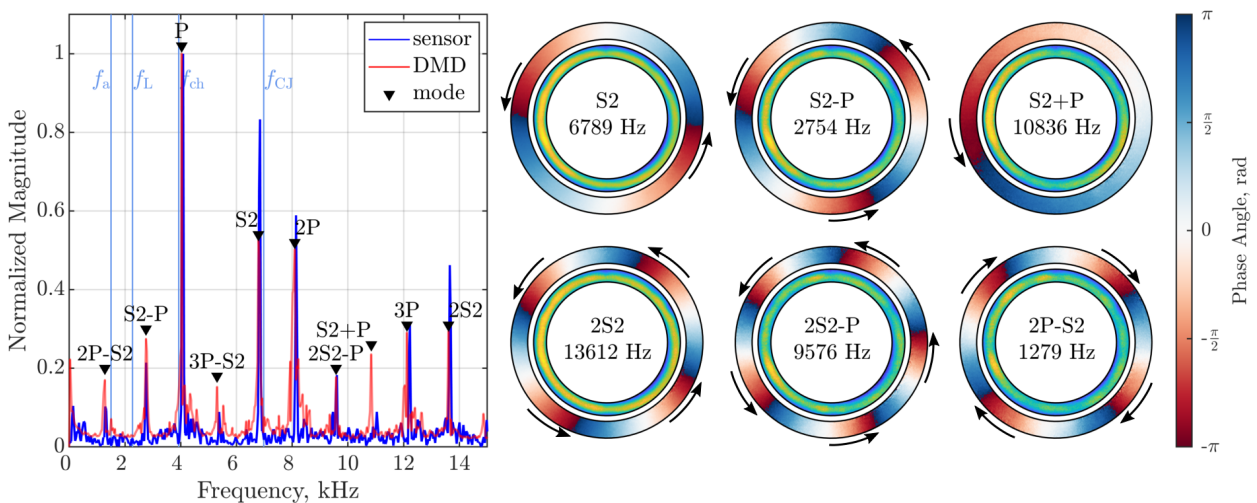


Figure 3: D/S2 mode at air mass flow of 250 g/s and equivalence ratio of 0.7: (left) DMD and pressure spectrum, and (right) corresponding mode phase (outer circle) and magnitude (inner circle).

When the mass flow is further increased, the RDC reaches stable operation with a dominant wave and a pair of counter-rotating waves. The corresponding spectra and mode shapes are shown in Fig. 3. Apart from the primary wave mode P (rotating clockwise, not shown), the spectra show a second large peak (labeled S2) below the second higher harmonic of P that has a large contribution in the pressure spectrum. Based on the mode shape and the video, it can be identified as a pair of counter-rotating waves propagating in counter-clockwise direction, denoted as S2. Its presence leads to a number of superposition modes with the primary wave. The speed of the wave intersection points is found at the difference between S2 and P. Since S2 is degenerate, the intersection point occurs twice per rotation of the primary wave, rotates in the direction of S2 and is found at a frequency of S2-P. Following the same logic as before, the mode shows three nodes. Contrary to the previous example, here the intersection mode S2+P shows a counter-clockwise rotating single-node mode. This might be due to a decreased impact of the intersection on P, as it is much stronger here. As a result, the mode likely shows the amplification of S2 from the wave intersection. Similar to the work shown in Xia et al. [2] the relative strengths of the two waves have an impact on how they evolve after intersection. The peak height of S2+P in the DMD spectrum is much higher compared to the pressure spectrum, suggesting that the luminosity increase captured here is an after-effect of wave intersection above

the sensor plane. The higher harmonic of S2 (denoted as 2S2) is found at twice the wave speed of S2 and, consistent with previous observations, shows a mode shape with twice as many nodes propagating in the same direction as S2. Also this mode appears to lead to a superposition mode with the primary wave, found close to 2S2-P. Following the same logic, another superposition mode is found close to 2P-S2. The role and importance of these superposition modes will be the topic of future investigations.

4 Conclusion

This work demonstrated the first successful application of the Dynamic Mode Decomposition (DMD) analysis to the aft-end view of rotating detonation waves in Rotating Detonation Combustors (RDCs). The method was applied to extract the dominant dynamic behavior captured in the high-speed videos imaged from the aft end of an RDC. Three different global operating modes with two counter-rotating waves at equal and different speeds, and with a dominant wave and a pair of counter-rotating waves were analyzed. The DMD spectrum was found to align well with the pressure spectrum recorded in the combustor annulus. The DMD modes confirmed the existence of a variety of superposition modes as a result of wave interaction and showed a dependence on the relative strengths of the waves. The DMD also confirmed the presence of a longitudinal wave mode related to a quarter-wave acoustic resonance driven by the annulus length. The DMD analysis has proven a valuable tool to analyze RDC operation and will be applied to further study the complex wave modes found here.

References

- [1] K. Kailasanath, "Recent developments in the research on rotating-detonation-wave engines," in *55th AIAA Aerospace Sciences Meeting*, p. 0784, 2017.
- [2] Z. Xia, X. Tang, M. Luan, S. Zhang, Z. Ma, and J. Wang, "Numerical investigation of two-wave collision and wave structure evolution of rotating detonation engine with hollow combustor," *International Journal of Hydrogen Energy*, vol. 43, no. 46, pp. 21582–21591, 2018.
- [3] V. Anand, A. St. George, R. Driscoll, and E. Gutmark, "Longitudinal pulsed detonation instability in a rotating detonation combustor," *Experimental Thermal and Fluid Science*, vol. 77, pp. 212–225, 2016.
- [4] R. Bluemner, M. D. Bohon, H.-Q. Nguyen, C. O. Paschereit, and E. J. Gutmark, "Influence of reactant injection parameters on RDC mode of operation," in *57th AIAA Aerospace Sciences Meeting*, 2019.
- [5] P. J. Schmid, "Dynamic mode decomposition of numerical and experimental data," *Journal of Fluid Mechanics*, vol. 656, pp. 5–28, 2010.
- [6] L. Massa, R. Kumar, and P. Ravindran, "Dynamic mode decomposition analysis of detonation waves," *Physics of Fluids*, vol. 24, no. 6, p. 066101, 2012.
- [7] J. H. Tu, C. W. Rowley, D. M. Luchtenburg, S. L. Brunton, and J. N. Kutz, "On dynamic mode decomposition: theory and applications," *Journal of Computational Dynamics*, no. 1(2), pp. 391–421, 2014.
- [8] M. D. Bohon, R. Bluemner, C. O. Paschereit, and E. J. Gutmark, "High-speed imaging of wave modes in an RDC," *Experimental Thermal and Fluid Science*, vol. 102, pp. 28–37, Apr. 2019.
- [9] R. Bluemner, M. D. Bohon, C. O. Paschereit, and E. J. Gutmark, "Dynamics of counter-rotating wave modes in an RDC," in *54th AIAA/SAE/ASEE Joint Propulsion Conference*, 2018.